Qubit-qubit entanglement mediated by epsilon-near-zero waveguide reservoirs

Ibrahim Issah[1] and Humeyra Caglayan[1]
Faculty of Engineering and Natural Science, Photonics, Tampere University, 33720 Tampere, Finland.

(* Author to whom correspondence should be addressed: humeyra.caglayan@tuni.fi)

(Dated: 14 December 2021)

This work investigates qubit entanglement in rolled-up and plasmonic rectangular epsilon-near-zero (ENZ) waveguide reservoirs. We explore the robust entanglement of qubits coupled to these reservoirs using the concurrence metric formalism and the emergence of driven steady-state entanglement under continuous pumping. The results indicate that the proposed rolled-up ENZ waveguide shows a high long-range entanglement of qubits embedded within as compared to the rectangular ENZ waveguide channel.

Entanglement or non-separability of qubits is relevant in quantum cryptography, quantum teleportation, and other two-qubit quantum processes[1–4]. Entanglement, which was initially used in systems such as optics, atoms, and ions, is becoming increasingly accessible in quantum physics[5,6]. Short distance entanglement, in particular, has been realized for spin degrees of freedom in quantum dots, nanotubes, or molecules[7–9]. However, long-range qubit-qubit interactions are required for long-distance information transfer. As a result, the correlation between the two qubits could be mediated by a reservoir composed of artificially engineered metamaterials that can support unique virtual bosons.

Metamaterial formations are one of the prominent engineering techniques that help to explore the classical, semi-classical, and quantum phenomena in the nanoscale. They are coined as tailoring the optical properties of a material to the desired value by designing its subwavelength nanostructures that help in attaining interesting optical phenomena[10,11]. From its inception, numerous techniques have been implemented to study their unique optical properties[12–16]. In particular, epsilon-near-zero (ENZ) metamaterials have been a material of interest due to their unique optical properties such as near-zero refractive index, decoupling of electricity and magnetism, large nonlinearity effect, and infinite phase velocity[17,18]. ENZ waveguides operating around its cutoff wavelength excites an effective zero-index mode. Typically, plasmonic waveguides excite unique extended ENZ modes at their corresponding cutoff wavelengths and can be integrated with quantum emitters to exhibit interesting atomic-field interactions. Numerical studies on rectangular ENZ reservoir[19,20] showed that ENZ mediums outperform the subwavelength distance limitations of qubits cooperative emission in a homogeneous medium. However, the difficulties to incorporate quantum emitters in a rectangular waveguide and their fabrication challenges in the nanoscale regime have hampered their practical use. As a result, achieving zero-index features necessitates a controlled and practical 3D manufacturing method. Rolled-up tubes have been shown to be easily fabricated using a self-rolling mechanism that could be practically utilized to incorporate emitters within[16,21–24]. Recently, Habib et al.[16] experimentally fabricated a cost-effective rolled-up tube composed of gold (Au) and SiO_2 using a self-rolling mechanism as compared to the rectangular ENZ waveguide with fabrication challenges[25]. These rolled-up waveguides have been shown to provide enhanced resonance energy transfer and good entanglement of qubits at their corresponding cutoff wavelength as compared to qubit-qubit cooperative emission in a homogeneous medium[26].

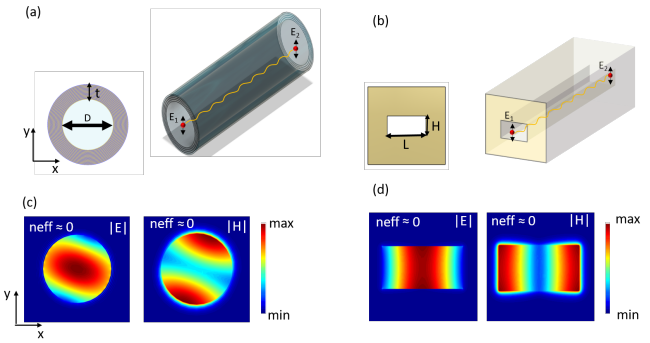

FIG. 1. Schematics of (a) rolled-up ENZ, and (b) rectangular ENZ waveguide with their corresponding cross-section in the x-y plane. E_1 and E_2 represents the two quantum emitters interacting with the corresponding ENZ waveguides. (c) The electric |E| and magnetic |H| fields of the fundamental TE_{11} mode (zero-index mode) of the rolled-up ENZ waveguide, and (d) the fundamental TE_{10} mode (zero-index mode) of the rectangular ENZ waveguide.

Here, we focus on rolled-up and rectangular ENZ waveguides serving as reservoirs to mediate qubit-qubit interactions at long distances and the emergence of driven steady-state entanglement under continuous double pumping. Based on these two experimentally proven ENZ waveguide channels, we numerically calculated their relations with quantum emitters when used as a quantum reservoir to determine the final state of a quantum system. We envisage that the different reservoirs seen by quantum emitters (qubits) will lead to different dyadic responses and, therefore, result in different long-range entanglements. Our study adopts ENZ waveguides into quantum systems which are foreseen to generate unique optical sources, durable entangled states, and other novel optical applications in different fields of study.

To determine the fundamental mode of the corresponding ENZ waveguide, numerical Finite Element EigenMode (FEEM) simulations were implemented in Ansys Lumerical

software to determine the cutoff wavelength of both the rolled-up and rectangular ENZ waveguide. Figure 1 illustrates the schematics (top panel) and field distributions (lower panel) (i.e. electric |E| and magnetic |H| fields) of the rolled-up and the rectangular ENZ waveguide. The numerically calculated fundamental modes of the proposed quantum reservoirs exhibit TE_{11} mode for the rolled-up ENZ waveguide with the existence of both radial and axial components of the transverse fields due to its symmetry as compared to the TE_{10} mode of the rectangular ENZ waveguide transverse to its propagation direction. The dimensions of the waveguides were set and optimized to attain the same cutoff wavelength of $\lambda_0 \approx 1400$ *nm*. The rolled-up ENZ waveguide has a diameter (D) of 700 *nm* and thickness (t) of 180 *nm* (i.e. 12 layers) with 5 *nm* of gold (Au) and 10 *nm* of SiO_2. The corresponding plasmonic (Au) rectangular ENZ waveguide has a dimension of 650×350 nm^2 (i.e. width (L) and height (H)), respectively.

Additionally, to confirm the obtained cutoff wavelength of the ENZ waveguide channels, we simulated the radiative power of a single qubit embedded within the waveguide as a function of different dipole positions and spectral wavelengths. Figure 2 corresponds to the total average power (W) emitted from the dipole (qubits) as a function of the dipole's axial position along the rolled-up and rectangular ENZ waveguide reservoirs at different orthogonal orientations (i.e. vertically and horizontally polarized). The heatmap of the rectangular waveguide shows dipole emission power above the cutoff wavelength due to its sharp edge effects compared to the rolled-up ENZ waveguide. The results show a uniform emitted power and hence a uniform decay rate enhancement along the axis of the waveguide at a cutoff wavelength of $\lambda_0 \approx 1400$ nm where the refractive index of the corresponding waveguide n ≈ 0. This zero-index medium exhibits a uniform field amplitude along the waveguide channel and is envisioned to mediate the long-range interaction of qubits embedded within these waveguide channels.

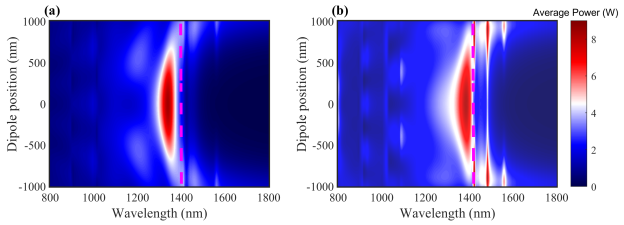

FIG. 2. Dipole emission average power (W) as a function of position along the (a) rolled-up waveguide and (b) rectangular waveguide at different spectral regions. The dash line represent the cutoff wavelength of the two ENZ waveguides.

After identifying the photonic properties of the ENZ waveguide channels, we initiated the entanglement calculations of qubits coupled with the corresponding ENZ reservoirs. Note that the measure of entanglement of qubits coupled to a reservoir[2,6] can be described by the concurrence C metric formalism by Wootters[27]. To determine the concurrence C metric formalism, it is pertinent to obtain the dyadic response of an emitter coupled to the rolled-up ENZ waveguide compared to the rectangular ENZ waveguide to determine their respective coupling parameters.

To start with, we considered two identical qubits with the same transition frequency ω_0 embedded within the aforementioned ENZ channels. The dynamic evolution of quantum systems coupled to lossy plasmonic environments is described by the dyadic Green's function in conjunction with the quantum master equation formalism. Note that the dyadic Green's function is a classical quantity used to study the spontaneous decay of quantum emitters coupled to a quantum reservoir. The quantum master equation describes the dynamics of the density matrix ρ of a two-qubit system near a reservoir. Assuming a weak excitation and weak coupling regime, the Born-Markov, and rotating wave approximations can be used to compute the master equation, which is expressed as [28]:

$$\frac{\partial \rho}{\partial t} = \frac{1}{i\hbar}[H,\rho] - \frac{1}{2}\sum_{i,j=1}^{2}\gamma_{ij}\left(\rho\sigma_i^{\dagger}\sigma_j + \sigma_i^{\dagger}\sigma_j\rho - 2\sigma_i\rho\sigma_j^{\dagger}\right) \tag{1}$$

where the Hamiltonian describing the coherent part of the evolutionary dynamics is expressed as:

$$H = \sum_i \hbar\left(\omega_0 + g_{ii}\right)\sigma_i^{\dagger}\sigma_i + \sum_{i\neq j}\hbar g_{ij}\sigma_i^{\dagger}\sigma_j \tag{2}$$

From Eqn. (1), ρ depicts the density matrix of the two-qubit system. $\sigma\left(\sigma^{\dagger}\right)$ represents the destruction (creation) operator applied to the qubits. The photonic Lamb shift g_{ii} due to the self-interaction of each qubit embedded within the ENZ waveguide is usually minimal and neglected in our formulations. g_{ij} also represents the coherent dipole-dipole interactions of the two identical qubits expressed as:

$$g_{ij} = \left(\omega_0^2/\varepsilon_0\hbar c^2\right)\mathrm{Re}\left[\boldsymbol{\mu}_i^* \cdot \mathbf{G}\left(\mathbf{r}_i,\mathbf{r}_j,\omega_0\right)\cdot\boldsymbol{\mu}_j\right], \tag{3}$$

where the dyadic Green's tensor $\mathbf{G}\left(\mathbf{r}_i,\mathbf{r}_j,\omega_0\right)$ satisfies the classical electromagnetic equations for a point dipole source located at a position $\mathbf{r}_j$.

Also, γ_{ij} represents the dissipative and noncoherent term of the master equation which is expressed as a function of the imaginary part of the dyadic Green's function:

$$\gamma_{ij} = \left(2\omega_0^2/\varepsilon_0\hbar c^2\right)\mathrm{Im}\left[\boldsymbol{\mu}_i^* \cdot \mathbf{G}\left(\mathbf{r}_i,\mathbf{r}_j,\omega_0\right)\cdot\boldsymbol{\mu}_j\right]. \tag{4}$$

To solve the master equation and to obtain the density matrix, a convenient basis for the two-qubit system vector space must be defined. It is easier to work in the Dicke basis: $|3\rangle = |e_1\rangle\otimes|e_2\rangle = |e_1,e_2\rangle$, $|0\rangle = |g_1\rangle\otimes|g_2\rangle = |g_1,g_2\rangle$, and $|\pm\rangle = 1/\sqrt{2}\left(|e_1,g_2\rangle \pm |g_1,e_2\rangle\right)$, when studying identical emitters in equivalent positions, i.e. $\gamma_{11} = \gamma_{22} = \gamma$, where, $|e_i\rangle$ ($|g_i\rangle$) represents the excited (ground) state of the i -th qubit. The basis selected is appropriate to characterize the response of the two-qubit system since it leads to a diagonalized Hamiltonian. In general, the entanglement between two qubits can be quantified by computing the concurrence C introduced by Wootters[27] expressed as:

$$C = \max\left(0, \sqrt{u_1} - \sqrt{u_2} - \sqrt{u_3} - \sqrt{u_4}\right), \tag{5}$$

where u_i represents the eigenvalues of the matrix $\rho\tilde{\rho}$. $\tilde{\rho} = \sigma_y\otimes\sigma_y\rho^*\sigma_y\otimes\sigma_y$ is the spin-flip density matrix and σ_y is

the Pauli matrix. The degree of concurrence is determined between 1 (completely entangled state) and 0 (unentangled state). However, to gain insight about the entanglement process between two emitters when only one of the emitter is excited, a transient concurrence formulation can be derived from the master equation which is expressed as:

$$C(t) = 0.5\sqrt{\left[e^{-(\gamma+\gamma_{12})t} - e^{-(\gamma-\gamma_{12})t}\right]^2 + 4e^{-2\gamma t}\sin^2(2g_{12}t)} \tag{6}$$

Note that the pure dephasing term γ' normally part of Eqn. (6)[2] is considered to be relatively small compared to the radiative decay rate of qubits coupled to an ENZ structure at low temperatures[29,30]. Thus, its contribution is insubstantial and considered as zero in our formulation. Interestingly, Vovcenko et al.[30] has recently showed that higher dephasing contributes to entanglement. Thus, dephasing is not only linked to the relaxation of the non-diagonal terms of the density matrix but can potentially lead to transitions between super- and sub-radiant states, thereby, leading to entangled states. Also, from Eqn. (6), $C(0) = 0$, since at $t = 0$, the quantum system is initially at an unentangled state. As time progresses, $t > 0$, the concurrence becomes larger than zero, meaning that the emitters become entangled. However, at some point the concurrence starts to decay with time and becomes zero again, $C(t) = 0$, after a long period of time ($t \to \infty$). Thus, the system needs to be sustained by an external source to prolong the entanglement.

External pumps with the same frequency (ω_p) can, therefore, be used to pump each emitter embedded within the ENZ waveguide channels, to prevent the transient concurrence from decaying after some time and to achieve steady-state entanglement. In that case, an additional term $1/i\hbar[V,\rho]$ needs to be introduced in the right-hand side of the quantum master equation, where the operator:

$$V = -\sum_{i}^{2}\hbar\left(\Omega_i e^{-i\Delta_i t}\sigma_i^{\dagger} + \Omega_i^{*} e^{i\Delta_i t}\sigma_i\right) \tag{7}$$

characterizes the interaction between the pump field and the emitter. The parameter $\Omega_i = \mu \cdot E_{0i}/\hbar$ is the effective Rabi frequency of the pump that depends on the induced electromagnetic field E_{0i} from the optical source pumping the i -th qubit. The parameter $\Delta_i = \omega_0 - \omega_p$ is the detuning parameter due to the pump frequency ω_p. After expressing ρ in the usual basis $|e_1,e_2\rangle, |e_1,g_2\rangle, |g_1,e_2\rangle$, and $|g_1,g_2\rangle$, one can calculate the steady-state concurrence C_{ss} by solving numerically the master equation where the Rabi frequency and detuning parameter due to the external pumping have been included.

From the above theory, we numerically compute the dyadic Green's response of a single emitter coupled to the ENZ waveguide channels. From the dyadic Green's function, we obtain the decay rate ($\gamma_{1,2}$) and dipole-dipole coupling interactions (g_{12}) of the qubit coupled to the waveguide channels. These coupling parameters (i.e. γ_{12}, g_{12}) are used in the quantum master equation to determine the evolutionary dynamics of the quantum system. Figure 3 (a) and (b) illustrates the normalized decay rate γ_{12}/γ and the dipole-dipole interactions g_{12}/γ of qubits coupled to the rolled-up ENZ waveguide and the rectangular ENZ waveguide channels, respectively. We obtain that the decay rate of the rectangular ENZ waveguide is faster as compared to the rolled-up ENZ waveguide. It can be seen that the decay rate of the rolled-up ENZ waveguide exceeds a normalized interatomic distance r_{12}/λ_0 of 1.5 before it goes to zero as compared to the rectangular ENZ waveguide. Due to the high propagation and non-radiative losses of the rectangular waveguide as compared to the rolled-up ENZ waveguide, we see a faster decay rate $\gamma_{12}/\gamma = 0$ at normalized interatomic distance $r_{12}/\lambda_0 < 1.5$. Also, the normalized dipole-dipole interactions g_{12}/γ of the rolled-up ENZ waveguide increase appreciably above zero (0) at normalized interatomic emitter distance $r_{12}/\lambda_0 < 0.5$ as compared to the rectangular waveguide. Both waveguide channels exhibit a monotonic decrease in the spontaneous decay rate γ_{12} and dipole-dipole coupling g_{12} as a function of normalized interatomic distance r_{12}/λ_0.

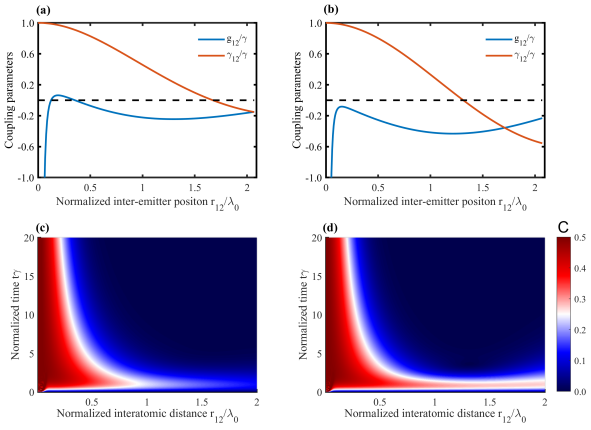

FIG. 3. Normalized decay rate enhancement γ_{12}/γ and dipole-dipole interaction g_{12}/γ as a function of normalized interatomic emitter distance r_{12}/λ_0 of (a) rolled-up ENZ waveguide and (b) rectangular waveguide. Measure of entanglement as a function of concurrence C for (c) rolled-up ENZ tube and (d) rectangular ENZ waveguide.

After identifying the coupling parameters relevant for the quantum master equation, we compute the concurrence C metric measure of entanglement as a function of normalized interatomic distance r_{12}/λ_0 and normalized evolution time $t\gamma$ as shown in Fig. 3 (c) and (d). We see relatively good transient concurrence C in both the rolled-up ENZ waveguide shown in Fig. 3 (c) and the rectangular waveguide presented in Fig. 3 (d). However, in both cases, we see a decrease in the concurrence as a function of time t which depicts the depopulation of emitters in the excited state due to both radiative and non-radiative losses. Typically, electron-phonon, ohmic loss, inherent losses of the excited ENZ mode, and propagation losses contribute to the transient nature of qubits entanglement mediated by an ENZ medium[20]. Also, the qubit-qubit dissipative coupling induces modified collective decay rates i.e., superradiant $\gamma+\gamma_{12}$ and subradiant states $\gamma-\gamma_{12}$ which exhibits pure superradiant emission when $\gamma = \gamma_{12}$ condition is satisfied[29].

In order to compensate for the depopulation of the emitter excited state, we introduce an external pump into the master

equation to compute the steady-state concurrence C_{ss} as well as the population dynamics of the qubits. Figure 4 shows the population dynamics of the qubits embedded within the two ENZ reservoirs at a normalized interatomic distance $r_{12}/\lambda_0 = 0.5$. Figure 4 (a), (c), and (e) illustrates the population dynamics of qubits inside the rolled-up ENZ waveguide at different pump intensities (i.e. antisymmetric $\Omega_1 = 0.8\gamma, \Omega_2 = 0$, symmetric $\Omega_1 = \Omega_2 = 0.5\gamma$, and asymmetric $\Omega_1 = -\Omega_2 = 0.5\gamma$ pumping cases). The corresponding Fig. 4 (b), (d), and (f) shows similar dynamics for qubits embedded within a plasmonic rectangular waveguide reservoir.

We present here four density matrix elements ρ_{gg}, ρ_{ee}, ρ_{ge}, and ρ_{eg}, which represent the probability of both qubits to be in the ground state, both qubits being in the excited state, the first qubit being in the ground state and the second being in the excited state, and vice versa. Furthermore, we assumed an initial state $\rho_{eg} = 1$. It can be seen that the qubits embedded within the ENZ reservoirs show different population dynamics for different external pumping cases. The symmetric pumping case depicts a similar population steady-state $\rho_{eg} = \rho_{ge}$ due to the identical pumping of the quantum system. The antisymmetric and asymmetric pumping density elements grow appreciably at normalized time $t\gamma < 5$ and decays to a constant probability at normalized time $t\gamma > 5$. Yet, we obtained a weak population state in the symmetric pumping case, for both rolled-up ENZ waveguide and plasmonic ENZ reservoir, as shown in Fig. 4 (c) and (d), respectively. At a high antisymmetric pumping case, we obtain an appreciable high probability of both qubits being in the excited state ρ_{ee} as compared to the other two coherent pump cases.

The high probability signifies the effect of strong pumping on the dynamics of emitters coupled to a reservoir and how it affects entanglement between two qubits. It is evident that under strong pumping, the dynamics of qubits are defined by the external pumps and not only by the dipole-dipole interactions, thereby affecting the entanglement of qubits in such vicinity. In the asymmetric pump case, we see a high population state $\rho_{eg} > \rho_{ge}$ of the first qubit since the pump intensity for the second qubit is negated. The aforementioned dynamics of the different pump scenarios show the effect of pump intensities on emitters' interactions and how high coherent pump intensities could potentially affect the entanglement property of qubits embedded within an ENZ reservoir with similar behavior observed with incoherent pumping[31,32].

Figure 5 also illustrates the heatmaps of steady-state concurrence C_{ss} at normalized evolution time $t\gamma = 90$ as a function of two normalized pump intensities (i.e. Ω_1/γ, Ω_2/γ) at different normalized interatomic distances r_{12}/λ_0. It is evident that the steady-state concurrence of the rolled-up ENZ waveguide (in the top panel of Fig. 5 (a), (b), (c)) shows a high measure of entanglement ($\max(C_{ss}) \approx 0.32$) as compared to the rectangular ENZ waveguide ($\max(C_{ss}) \approx 0.2$) shown in the lower panel (i.e. (d), (e), (f)) at $r_{12}/\lambda_0 = 0.5$. Similar results are presented for different normalized interatomic distances $r_{12}/\lambda_0 = 1.0$ and $r_{12}/\lambda_0 = 1.5$ respectively. The high entanglement in the rolled-up ENZ waveguide depicts its relevance to serve as a reservoir to mediate qubit entanglement as compared to the rectangular ENZ waveguide. Note that the

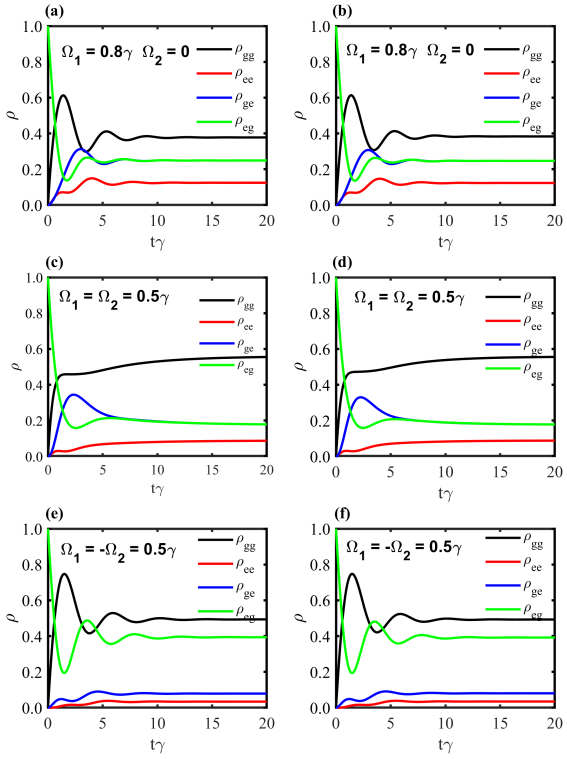

FIG. 4. Dynamics of the density matrix elements for qubits under external pumping. (a), (c), and (e) Population dynamics of qubits inside the rolled-up ENZ waveguide. (b), (d), and (f) Similar dynamics of qubits inside the plasmonic rectangular waveguide at different pump intensities.

high steady-state concurrence of the proposed ENZ waveguide channels is as a result of the large values of γ_{12} and small values of g_{12}. Also, the pump strength should not be too high to achieve strong steady-state entanglement between the qubits; otherwise, strong interactions between the pump and the qubits as well as the reservoir will occur, eventually leading to qubits decoupling and lasing.

To conclude, we have shown the long-range quantum entanglement between a pair of qubits mediated by a rolled-up ENZ waveguide, which persists over extended periods and long distances. The response is compared to the corresponding plasmonic rectangular ENZ waveguide. The theory of both transient and steady-state quantum entanglement, quantified by computing the concurrence metric, is briefly introduced, and utilized to determine the robust entanglement of qubits coupled to the ENZ waveguide channel. This concurrence metric formalism has a direct link with the cross-term second-order coherence function that can be extracted from an experiment (i.e., Hanbury Brown and Twiss (HBT) effect or two-photon detection probability (PRR) measurement)[20,29,33]. We also showed ways to improve the entanglement of qubits coupled to the proposed reservoirs. We obtain that the rolled-up ENZ waveguide system demonstrates an improved quantum opti-

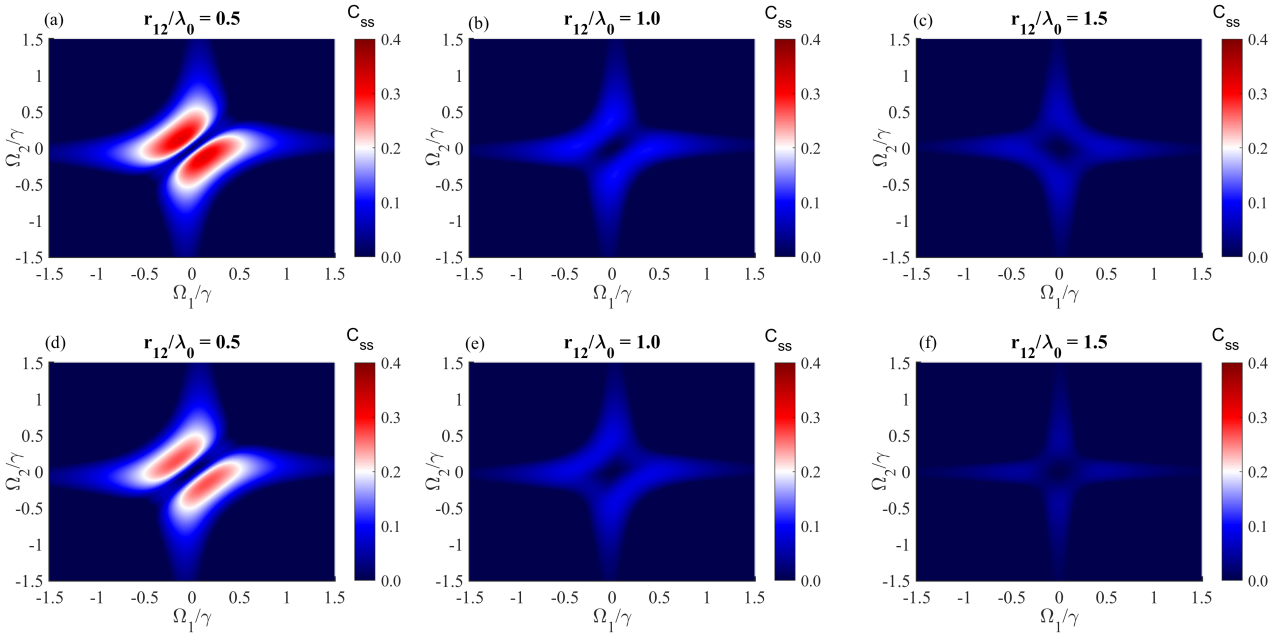

FIG. 5. Two pumps steady-state entanglement at different inter-atomic distance r_{12}/λ_0 for (top panel) rolled-up ENZ waveguide and (bottom panel) rectangular waveguide.

cal and long-range entanglement performance with max(C_{ss}) ≈ 0.32 compared to the rectangular ENZ waveguide channel. This study could open new avenues to explore entanglement for quantum network applications, quantum information processing, cryptography, and the development of ultra-sensitive sub-wavelength metrology devices.

ACKNOWLEDGMENTS

We acknowledge the financial support of the European Research Council (Starting Grant project aQUARiUM; Agreement No. 802986), Academy of Finland Flagship Programme, (PREIN), (320165).

DATA AVAILABILITY STATEMENT

The data that support the findings of this study are available from the corresponding author upon reasonable request. The version of the codes used to generate the concurrence calculations are provided here: https://github.com/issahi62/Rolled-up-ENZ-Waveguide and users of these codes are kindly requested to cite its use in their work.

[1] M. O. Scully and M. S. Zubairy, *Quantum Optics* (Cambridge University Press, 1997).
[2] S. A. H. Gangaraj, A. Nemilentsau, G. W. Hanson, and S. Hughes, "Transient and steady-state entanglement mediated by three-dimensional plasmonic waveguides," Optics Express **23**, 22330 (2015).
[3] S. A. H. Gangaraj, G. W. Hanson, and M. Antezza, "Robust entanglement with three-dimensional nonreciprocal photonic topological insulators," Physical Review A **95**, 063807 (2017).
[4] P. Kok, "Principles of quantum computation and information volume II," Journal of Physics A: Mathematical and Theoretical **40** (2007), 10.1088/1751-8121/40/40/b03.
[5] Y. Hao and G.-L. Long, "Quantum information and quantum computing," Fundamental Research **1** (2021), 10.1016/j.fmre.2021.01.007.
[6] A. Gonzalez-Tudela, D. Martin-Cano, E. Moreno, L. Martin-Moreno, C. Tejedor, and F. J. Garcia-Vidal, "Entanglement of two qubits mediated by one-dimensional plasmonic waveguides," Physical Review Letters **106**, 020501 (2011).
[7] Y. Makhlin, G. Schön, and A. Shnirman, "Quantum-state engineering with Josephson-junction devices," Reviews of Modern Physics **73** (2001), 10.1103/RevModPhys.73.357.
[8] R. Hanson, L. P. Kouwenhoven, J. R. Petta, S. Tarucha, and L. M. Vandersypen, "Spins in few-electron quantum dots," Reviews of Modern Physics **79** (2007), 10.1103/RevModPhys.79.1217.
[9] B. Lienhard, T. Schröder, S. Mouradian, F. Dolde, T. T. Tran, I. Aharonovich, and D. Englund, "Bright and photostable single-photon emitter in silicon carbide," Optica **3** (2016), 10.1364/optica.3.000768.
[10] Y. Liu and X. Zhang, "Metamaterials: A new frontier of science and technology," Chemical Society Reviews **40**, 2494–2507 (2011).
[11] Y. Li and C. Argyropoulos, "Controlling collective spontaneous emission with plasmonic waveguides," Optics Express **24**, 26696 (2016).
[12] M. A. Noginov, H. Li, Y. A. Barnakov, D. Dryden, G. Nataraj, G. Zhu, C. E. Bonner, M. Mayy, Z. Jacob, and E. E. Narimanov, "Controlling spontaneous emission with metamaterials," Optics Letters **35**, 1863 (2010).
[13] T. Tumkur, G. Zhu, P. Black, Y. A. Barnakov, C. E. Bonner, and M. A. Noginov, "Control of spontaneous emission in a volume of functionalized hyperbolic metamaterial," Applied Physics Letters **99**, 151115 (2011).
[14] J. Kerbst, S. Schwaiger, A. Rottler, A. Koitmäe, M. Brll, J. Ehlermann, A. Stemmann, C. Heyn, D. Heitmann, and S. Mendach, "Enhanced transmission in rolled-up hyperlenses utilizing Fabry-Pérot resonances," Applied Physics Letters **99**, 191905 (2011).
[15] D. R. Smith, D. C. Vier, T. Koschny, and C. M. Soukoulis, "Electromagnetic parameter retrieval from inhomogeneous metamaterials," Physical Review E - Statistical, Nonlinear, and Soft Matter Physics **71**, 036617 (2005).
[16] M. Habib, I. Issah, D. Briukhanova, A. R. Rashed, and H. Caglayan, "Wavefront Control with Nanohole Array-Based Out-of-Plane Metasurfaces," ACS Applied Nano Materials **16**, 28 (2021).

[17] E. J. Smith, Z. Liu, Y. Mei, and O. G. Schmidt, "Combined surface plasmon and classical waveguiding through metamaterial fiber design," Nano Letters **10**, 1–5 (2010).

[18] B. Edwards, A. Alù, M. E. Young, M. Silveirinha, and N. Engheta, "Experimental verification of epsilon-near-zero metamaterial coupling and energy squeezing using a microwave waveguide," Physical Review Letters **100**, 033903 (2008).

[19] R. Sokhoyan and H. A. Atwater, "Quantum optical properties of a dipole emitter coupled to an ε-near-zero nanoscale waveguide," Opt. Express **21**, 32279–32290 (2013).

[20] Y. Li, A. Nemilentsau, and C. Argyropoulos, "Resonance energy transfer and quantum entanglement mediated by epsilon-near-zero and other plasmonic waveguide systems," Nanoscale **11**, 14635–14647 (2019).

[21] S. M. Harazim, W. Xi, C. K. Schmidt, S. Sanchez, and O. G. Schmidt, "Fabrication and applications of large arrays of multifunctional rolled-up SiO/SiO 2 microtubes," Journal of Materials Chemistry **22**, 2878–2884 (2012).

[22] E. Bermúdez-Ureña and U. Steiner, "Self-rolled multilayer metasurfaces," ACS Photonics **6**, 2198–2204 (2019).

[23] V. Y. Prinz, E. V. Naumova, S. V. Golod, V. A. Seleznev, A. A. Bocharov, and V. V. Kubarev, "Terahertz metamaterials and systems based on rolled-up 3D elements: designs, technological approaches, and properties," Scientific Reports (2017), 10.1038/srep43334.

[24] D. Briukhanova, M. Habib, I. Issah, and H. Caglayan, "Low loss fishnet metamaterial via self-rolled nanotechnology," Applied Physics Letters **119**, 141101 (2021), https://doi.org/10.1063/5.0063120.

[25] E. J. R. Vesseur, T. Coenen, H. Caglayan, N. Engheta, and A. Polman, "Experimental verification of n=0 structures for visible light," Physical Review Letters **110**, 013902 (2013).

[26] I. Issah, M. Habib, and H. Caglayan, "Long-range qubit entanglement via rolled-up zero-index waveguide," Nanophotonics (2021), 10.1515/nanoph-2021-0453.

[27] W. K. Wootters, "Entanglement of formation of an arbitrary state of two qubits," Physical Review Letters **80**, 2245–2248 (1998).

[28] H. T. Dung, L. Knöll, and D.-G. Welsch, "Resonant dipole-dipole interaction in the presence of dispersing and absorbing surroundings," Phys. Rev. A **66**, 063810 (2002).

[29] D. Martín-Cano, A. González-Tudela, L. Martín-Moreno, F. J. García-Vidal, C. Tejedor, and E. Moreno, "Dissipation-driven generation of two-qubit entanglement mediated by plasmonic waveguides," Phys. Rev. B **84**, 235306 (2011).

[30] I. V. Vovcenko, V. Y. Shishkov, and E. S. Andrianov, "Dephasing-assisted entanglement in a system of strongly coupled qubits," Opt. Express **29**, 9685–9698 (2021).

[31] E. del Valle, "Strong and weak coupling of two coupled qubits," Phys. Rev. A **81**, 053811 (2010).

[32] C. A. Downing, J. C. L. Carreño, A. I. Fernández-Domínguez, and E. del Valle, "Asymmetric coupling between two quantum emitters," Phys. Rev. A **102**, 013723 (2020).

[33] E. Özgün, E. Ozbay, and H. Caglayan, "Tunable Zero-Index Photonic Crystal Waveguide for Two-Qubit Entanglement Detection," ACS Photonics **3**, 2129–2133 (2016).